

# Three-dimensional cardiac fibre disorganization as a novel parameter for ventricular arrhythmia stratification after myocardial infarction

**Daniel G. León<sup>1†</sup>, Mariña López-Yunta<sup>2†</sup>, José Manuel Alfonso-Almazán<sup>1</sup>, Manuel Marina-Breyse<sup>1,3</sup>, Jorge G. Quintanilla<sup>1,4,5</sup>, Javier Sánchez-González<sup>6</sup>, Carlos Galán-Arriola<sup>1,5</sup>, Francisco Castro-Núñez<sup>1</sup>, Juan José González-Ferrer<sup>4,5</sup>, Borja Ibáñez<sup>1,5,7</sup>, Julián Pérez-Villacastín<sup>4,5,8</sup>, Nicasio Pérez-Castellano<sup>4,5</sup>, Valentín Fuster<sup>1,9</sup>, José Jalife<sup>1,5,10</sup>, Mariano Vázquez<sup>2</sup>, Jazmín Aguado-Sierra<sup>2</sup>, and David Filgueiras-Rama<sup>1,4,5\*</sup>**

<sup>1</sup>Centro Nacional de Investigaciones Cardiovasculares (CNIC), Myocardial Pathophysiology Area, Melchor Fernández Almagro 3, Madrid 28029, Spain; <sup>2</sup>Department of Computer Applications in Science and Engineering, Barcelona Supercomputing Center (BSC), Barcelona, Spain; <sup>3</sup>Agencia Española de Protección de la Salud en el Deporte (AEPSAD), Madrid, Spain; <sup>4</sup>Department of Cardiology, Instituto de Investigación Sanitaria del Hospital Clínico San Carlos (IdISSC), Cardiovascular Institute, Madrid, Spain; <sup>5</sup>CIBER de Enfermedades Cardiovasculares, Madrid, Spain; <sup>6</sup>Philips Healthcare Iberia, Madrid, Spain; <sup>7</sup>ILIS-University Hospital Fundación Jiménez Díaz, Madrid, Spain; <sup>8</sup>Fundación Interhospitalaria para la Investigación Cardiovascular (FIC), Madrid, Spain; <sup>9</sup>The Zena and Michael A. Wiener Cardiovascular Institute, Icahn School of Medicine at Mount Sinai, New York, NY, USA; and <sup>10</sup>Department of Internal Medicine, Center for Arrhythmia Research, Cardiovascular Research Center, University of Michigan, Ann Arbor, MI, USA

Received 28 July 2018; editorial decision 30 November 2018; accepted 3 December 2018; online publish-ahead-of-print 12 January 2019

## Aims

Myocardial infarction (MI) alters cardiac fibre organization with unknown consequences on ventricular arrhythmia. We used diffusion tensor imaging (DTI) of three-dimensional (3D) cardiac fibres and scar reconstructions to identify the main parameters associated with ventricular arrhythmia inducibility and ventricular tachycardia (VT) features after MI.

## Methods and results

Twelve pigs with established MI and three controls underwent invasive electrophysiological characterization of ventricular arrhythmia inducibility and VT features. Animal-specific 3D scar and myocardial fibre distribution were obtained from ex vivo high-resolution contrast-enhanced T1 mapping and DTI sequences. Diffusion tensor imaging-derived parameters significantly different between healthy and scarring myocardium, scar volumes, and left ventricular ejection fraction (LVEF) were included for arrhythmia risk stratification and correlation analyses with VT features. Ventricular fibrillation (VF) was the only inducible arrhythmia in 4 out of 12 infarcted pigs and all controls. Ventricular tachycardia was also inducible in the remaining eight pigs during programmed ventricular stimulation. A DTI-based 3D fibre disorganization index (FDI) showed higher disorganization within dense scar regions of VF-only inducible pigs compared with VT inducible animals (FDI: 0.36; 0.36–0.37 vs. 0.32; 0.26–0.33, respectively,  $P=0.0485$ ). Ventricular fibrillation induction required lower programmed stimulation aggressiveness in VF-only inducible pigs than VT inducible and control animals. Neither LVEF nor scar volumes differentiated between VF and VT inducible animals. Re-entrant VT circuits were localized within areas of highly disorganized fibres. Moreover, the FDI within heterogeneous scar regions was associated with the median VT cycle length per animal ( $R^2=0.5320$ ).

\* Corresponding author. Tel: +34 91 4531200 (ext: 1510); fax: +34 91 4531265. E-mail address: david.filgueiras@cnic.es

† The first two authors contributed equally to this study.

© The Author(s) 2019. Published by Oxford University Press on behalf of the European Society of Cardiology.

This is an Open Access article distributed under the terms of the Creative Commons Attribution Non-Commercial License (<http://creativecommons.org/licenses/by-nc/4.0/>), which permits non-commercial re-use, distribution, and reproduction in any medium, provided the original work is properly cited. For commercial re-use, please contact [journals.permissions@oup.com](mailto:journals.permissions@oup.com)

**Conclusion**

The amount of scar-related cardiac fibre disorganization in DTI sequences is a promising approach for ventricular arrhythmia stratification after MI.

**Keywords**

Cardiac fibres • Diffusion tensor imaging • Arrhythmia stratification • Myocardial infarction • Magnetic resonance imaging

**What's new?**

- High-resolution *ex vivo* cardiac magnetic resonance (CMR) sequences demonstrated that diffusion tensor imaging (DTI) properties differ between healthy and scar areas after established myocardial infarction (MI) in the pig model.
- Animal-specific three-dimensional (3D) cardiac fibre reconstruction showed that a novel DTI-based fibre disorganization index (FDI) properly differentiated between ventricular tachycardia (VT) inducible animals and ventricular fibrillation (VF)-only inducible animals, despite VF-only inducible animals required lower programmed stimulation aggressiveness.
- Re-entrant VT circuits were localized within areas of highly disorganized fibres detected by DTI and mainly composed of viable myocardium. Fibre disorganization within heterogeneous scar regions also correlated with the median animal-specific VT cycle length.
- High-resolution CMR-derived scar volumes did not associate with either VT features or VF inducibility.
- Scar-related cardiac fibre disorganization obtained from a DTI-based 3D FDI has the potential to improve ventricular arrhythmia risk stratification after established MI.

Some groups have also addressed the potential relevance of viable surviving myocardial fibres in establishing substrate-sensitive re-entrant activity and ventricular arrhythmia.<sup>4</sup> Spatial fibre arrangement and local curvature within the infarct area seem to be important in establishing a re-entrant circuit leading to ventricular tachycardia (VT).<sup>8</sup> Diffusion tensor imaging (DTI) is an emerging technique for non-invasive reconstruction of the cardiac fibre architecture based on water diffusion properties.<sup>9</sup> In fact, *ex vivo* DTI has been proven to be greatly reproducible in the assessment of myocardial microstructure,<sup>9,10</sup> whereas *in vivo* implementation remains a challenge affected by technical difficulties, including intrinsic motion and poor resolution.<sup>9</sup>

*In vivo* limitations to integrate fibre organization with scar distribution using CMR and further assessment of ventricular arrhythmia risk and VT features could be overcome using a well-described pig model of infarct-related VT.<sup>4,8</sup> We hypothesize that DTI-derived cardiac fibre properties modulate the arrhythmia risk and VT features after MI. We aimed to: (i) establish DTI-derived parameters detecting structural differences between scar and healthy regions, and (ii) study the implications of high-resolution scar characterization and myocardial fibre disorganization in ventricular arrhythmia inducibility and VT features after MI.

**Introduction**

Risk stratification of ventricular arrhythmia after myocardial infarction (MI) is one of the missing links in evidence-based MI management identified in the most recent guidelines.<sup>1</sup> Despite its lack of specificity, left ventricular ejection fraction (LVEF) remains the main factor for risk stratification of sudden cardiac death after MI.<sup>2</sup>

Pathophysiological changes in the infarct region include myocyte loss and replacement of the extracellular matrix with fibrosis, which establishes an intermingling of viable myocytes and collagen that settles a heterogeneous substrate with areas of potentially slow conduction leading to re-entrant ventricular arrhythmias.<sup>3,4</sup> Delayed gadolinium-enhanced cardiac magnetic resonance (LGE-CMR) enables the differentiation between areas of moderate and severe fibrosis, which allows scar characterization as intermediate signal intensity regions (heterogeneous scar) and elevated signal intensity regions (dense scar). Moreover, several studies have shown that scar tissue quantification using LGE-CMR may increase the predictive performance of inducible and spontaneous ventricular arrhythmia after MI,<sup>5</sup> although there is considerable overlap in scar size between patients with and without ventricular arrhythmia.<sup>6,7</sup> Nonetheless, the predictive value of CMR-based scar characterization remains controversial and has not been incorporated as a standard stratification tool in clinical practice.<sup>2</sup>

**Methods****Pig model of myocardial infarction**

The studies were conducted in accordance with institutional guidelines and Spanish and European regulation guidelines for the care and use of laboratory animals. All CMR studies and interventional procedures were performed under general anaesthesia (see [Supplementary material online](#)). In brief, 16 male pigs (large-white strain, ~35 kg) underwent catheterization of the left anterior descending (LAD) coronary artery using percutaneous femoral access and fluoroscopic guidance. An angioplasty balloon was positioned and inflated either proximal or distal to the first diagonal branch of the LAD in 10 and 6 animals, respectively (see [Supplementary material online, Table S1](#)), to generate different infarct sizes and variable scar distributions ([Figure 1A](#)). After 5 days of recovery, the animals were transferred to specialized animal research facilities for 10–12 weeks before CMR studies and invasive cardiac electrophysiology characterization. Four animals died suddenly before completing the 10- to 12-week period. A group of three additional weight-matched pigs with no MI were included as controls.

**Cardiac functional assessment and electrophysiology study**

All pigs underwent cardiac functional assessment 1-to-3 days before the electrophysiology study using a Philips Achieva 3T-Tx whole-body scanner (Philips Healthcare, Best, The Netherlands) ([Figure 1B](#)). Segmented

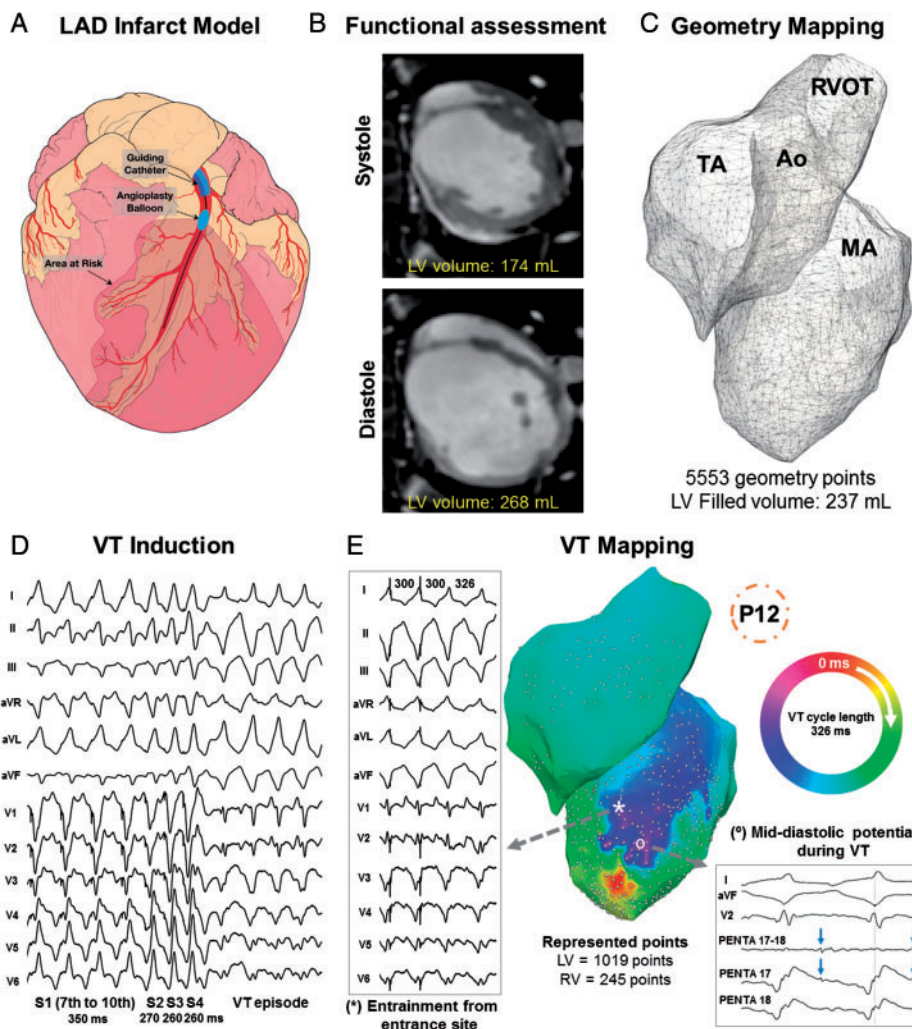


**Figure 1** Experimental workflow. (A) Schematic representation of the infarct model. (B) Functional cine assessment. (C) Endocardial ventricular geometry from the Carto3 electroanatomic mapping system. (D) Programmed ventricular stimulation for VT/VF induction. (E) Complete characterization of the re-entrant VT circuit by activation mapping and entrainment manoeuvres. Ao, aorta; LAD, left anterior descending coronary artery; LV, left ventricle; MA, mitral annulus; P12, pig ID number; RV, right ventricle; RVOT, right ventricular outflow tract; TA, tricuspid annulus; VF, ventricular fibrillation; VT, ventricular tachycardia.

and electrocardiogram-gated cine steady-state free precession was performed to acquire 11–13 contiguous short-axis slices covering the heart from the base to the apex to evaluate LVEF.

The invasive electrophysiology study was performed using percutaneous venous and arterial femoral access to reach the right (RV) and left (LV) ventricles. Additional epicardial access was achieved using a percutaneous subxiphoid approach. A screw-in catheter was positioned in the RV for programmed ventricular stimulation and a 24-pole catheter (Orbiter Woven, Boston Scientific, Queensbury, NY, USA) was positioned on the epicardium to simultaneously record atrial and ventricular electrograms. A 6-F pigtail catheter was also positioned in the aorta to monitor haemodynamic changes. The RV, LV, and the epicardial geometries were generated using the fast anatomical mapping technology of the Carto3 electroanatomic mapping system (Biosense Webster, Diamond Bar, CA) and a 3.5-mm irrigated-tip mapping catheter (Navistar Thermocool, Biosense Webster) (Figure 1C). Electrical and blood

pressure signals were continuously monitored using the LabSystem-Pro electrophysiology recording system (Boston Scientific, Lowell, MA, USA). Then, synchronized programmed right ventricular stimulation was initiated using up to five basic drive cycle lengths (BDCL; S1; 10 pacing beats) at 350, 300, 280, 260, and 250 ms. A maximum of four extrastimuli (S2, S3, S4, and S5) were included and progressively decremented in 10 ms steps until refractoriness or a 180 ms coupling interval. If VT or ventricular fibrillation (VF) was no inducible, the protocol included sequential burst pacing for 10 s at 240, 230, 220, 210, 200, and 180 ms BDCL. Detailed description of the stimulation protocol is included in the [Supplementary material online](#). Stimulation was delivered at twice the threshold capture (pulse width: 2 ms). If the arising VT was haemodynamically stable, VT activation maps and entrainment manoeuvres were performed to localize the re-entrant circuit using the 3.5-mm tip catheter or a 20-pole steerable mapping catheter (Pentaray, Biosense Webster) (Figure 1D, E and [Supplementary material online, Movie S1](#)). All inducible

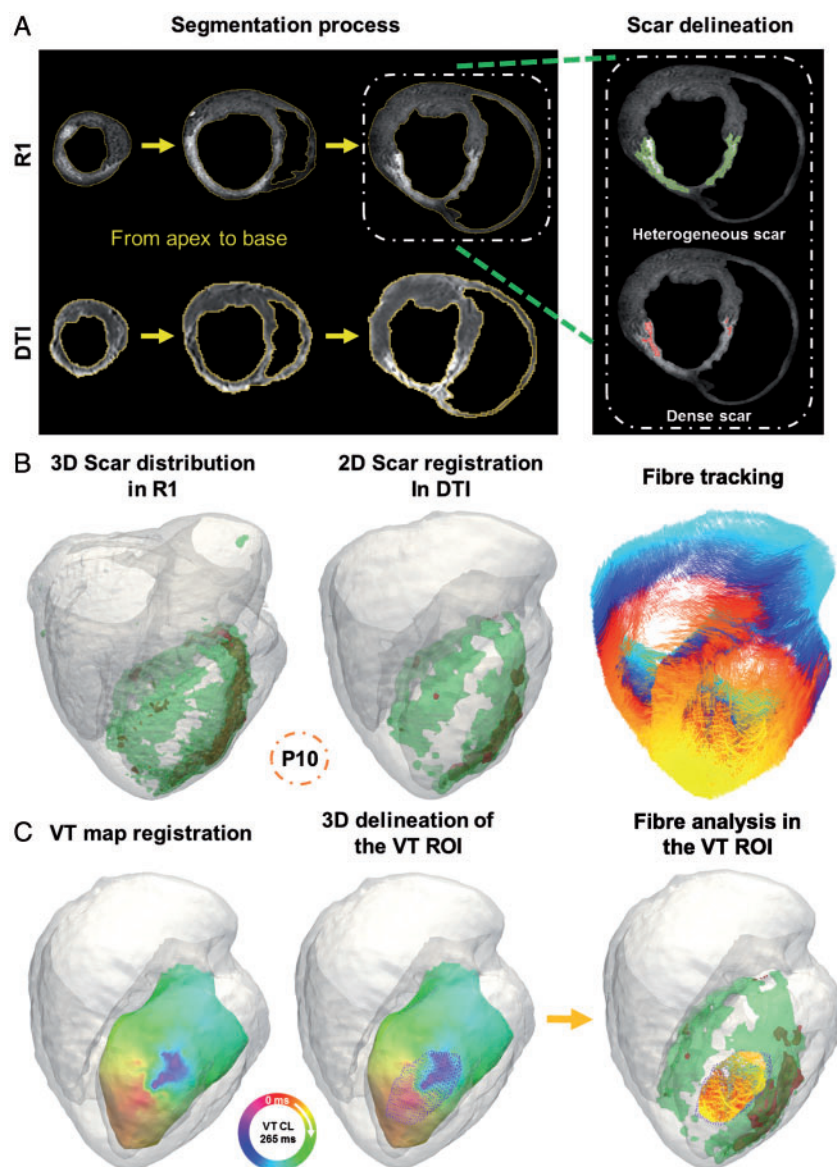


**Figure 2** Processing workflow. (A) Segmented short-axis slices from both R1 and DTI (b0) sequences, highlighting both heterogeneous (green) and dense (red) scar regions (right panel). (B) High-resolution R1-derived scar regions (on the left) were registered in the 3D DTI reconstruction using affine transformations (middle panel), yielding voxel-level structural analysis between healthy and scar regions. Then, cardiac tractography was generated using DTIStudio (right panel). The tracts are colour-coded using the long-axis 3D co-ordinates. (C) VT activation maps were registered onto the DTI geometry (left panel) and the VT ROI was detected (middle panel) to obtain a 3D VT ROI within the DTI reconstruction (right panel). This yielded further fibre and structural insights of the animal-specific VT. 3D, three-dimensional; DTI, diffusion tensor imaging; P10, pig ID number; ROI, region of interest; VT, ventricular tachycardia.

sustained monomorphic VT (SMVT) morphologies were registered and mapped if the tachycardia was haemodynamically stable. Acquired bipolar signals were filtered at 30–500 Hz and maps were stored for further processing. Direct current cardioversion was delivered to restore sinus rhythm in case of VF or haemodynamic collapse. Finally, a single intravenous bolus (0.2 mM/kg) of gadolinium-based contrast agent (Dotarem, Guerbet) was administered 10 min before euthanasia and heart excision. Offline signal processing and the sequential steps to calculate an aggressiveness index (AI) representing a relative score of the animal's sensitivity to VT or VF induction are described in the [Supplementary](#)

[material online and Figures S1, S2](#). Briefly, the AI was defined as the step number of the programmed stimulation protocol relative to the maximum number of steps.

### Magnetic resonance protocol

Right after euthanasia (intravenous sodium pentobarbital, 40 mg/kg) and heart excision, the hearts were prepared and filled with a 2% warm agarose gel solution to achieve volume-preserved heart conditions and avoid the collapse of cardiac chambers (see [Supplementary material online](#)).



Then, the heart was introduced in a custom-designed, watertight plastic flask containing 2% agarose gel and that perfectly adjusted to the eight-channel phased array knee coil (see [Supplementary material online, Figure S3](#)). The CMR sequences consisted of: (i) three-dimensional (3D) T1 mapping using a Look-Locker inversion recovery-turbo field echo sequence (TR/TE/Flip Angle = 5.9 ms/2.8 ms/7°) with acquired isotropic resolution of 0.6 mm<sup>3</sup>. Thirty-six inversion times were acquired with a 147-ms gap between them. New inversion pulses were applied every 6 s to ensure full signal recovery before consecutive pre-pulses. (ii) 2D DTI with a single-shot spin echo-planar imaging sequence (acquired isotropic resolution of 1.1 mm<sup>3</sup>), applying 15 different diffusion directions ( $b = 600$  s/mm<sup>2</sup>) plus the reference image ( $b = 0$  s/mm<sup>2</sup>).

## Image processing of cardiac magnetic resonance acquisitions

### R1 image processing

R1 images were calculated from the 36-inversion times of T1 images using a customized software (IDL 8.1, Boulder, CO, USA). Initial segmentation of the myocardium was performed semi-automatically using custom-made software in Matlab (MathWorks Inc., Natick, MA, USA), complemented with fine manual segmentation (~28–30 h per heart) ([Figure 2A](#)). Scar segmentation was performed based on the full-width-half-maximum method.<sup>11</sup> Signal intensity normalized to maximum myocardial signal intensity with cut-off values of 0.45 for heterogeneous scar and 0.67 for dense scar resulted in accurate scar segmentation (see [Supplementary material online, Figure S4](#)).<sup>12</sup> The final segmentation showed a median of <1% of remote heterogeneous scar (see [Supplementary material online, Figure S4](#)), which is compatible with mild fibrotic remodelling in remote areas.

### Diffusion tensor image processing

The DTI images were segmented semi-automatically and refined manually with a custom-made software and interface in Matlab ([Figure 2A](#)). R1-derived scar regions were registered in the DTI using affine transformations, providing delineated scar regions in the DTI sequence ([Figure 2B](#) and [Supplementary material online, Figure S5](#)). After the registration process, diffusion image voxels were clustered into healthy, heterogeneous, and dense regions. Diffusion tensor eigenvalues and eigenvectors, as well as tensor-derived parameters were calculated using DTIStudio.<sup>13</sup> Additional tensor-derived parameters (e.g. helix angles) were calculated using custom-made software in Matlab (see also [Supplementary material online](#)). We defined a new DTI parameter to quantify 3D regional structural disorganization; fibre disorganization index (FDI) as the cumulative 3D angle between the main direction of a given eigenvector and its neighbours (26 neighbours, radius 1), relative to a fixed maximum disorganization of 90° in each neighbouring eigenvector (see [Supplementary material online](#) for details).

### Cardiac fibre tracts processing

Cardiac fibres were generated in the full DTI segmentation volume using the Fast Assignment by Continuous Tracking (FACT) algorithm provided by DTIStudio.<sup>13</sup> In brief, the algorithm is fed by two diffusion tensor parameters: fractional anisotropy (FA) and fibre voxel-to-voxel turning angle. These parameters were used to find neighbouring voxels for every voxel and from any given voxel to construct a cardiac fibre. Generated fibre tracts were automatically associated to healthy myocardium, heterogeneous, and dense scar regions, based on prior scar registration in the DTI segmentation ([Figure 2B](#)).

## Three-dimensional processing of the ventricular tachycardia region of interest

Ventricular tachycardia activation maps in haemodynamically stable VTs were registered offline performing a landmark-based registration onto the DTI geometry using the aorta, mitral annulus and left ventricular apex as anatomical landmarks ([Figure 2C](#)). The VT region of interest (ROI) was defined as the area containing activation times varying up to a maximum of 10% of the VT cycle length (CL) from the earliest and latest activation times, respectively. Then, the VT ROI was projected on the DTI volume to obtain a 3D VT ROI within the DTI and 3D cardiac fibres distribution ([Figure 2C](#) and see [Supplementary material online](#)).

## Statistical analysis

Data are expressed as median and interquartile range (IQR) for quantitative variables, and number and percentage for qualitative variables. Data normality was assessed with the Anderson–Darling test (statistical significance;  $P < 0.01$ ). The Kruskal–Wallis *post hoc* test was applied to perform intra-case and inter-case comparisons for individual DTI parameters (statistical significance;  $P < 0.0001$ ). The Mann–Whitney *U* test was used for group comparisons. The Pearson's correlation coefficient ( $R^2$ ) was used for variable comparisons. A  $P$ -value of  $<0.05$  was considered statistically significant for both group and variable comparisons. All data were analysed in Graphpad Prism (GraphPad Software Inc., San Diego, CA, USA), except DTI group comparisons, which were analysed using custom-made software in Matlab.

## Results

Between September 2015 and January 2017, 12 pigs with MI and three weight-matched controls underwent complete invasive electrophysiology characterization and CMR studies. All baseline characteristics, scar volumes, VT, and VF features are summarized in [Table 1](#).

## Diffusion tensor imaging properties differ among healthy and scar regions

Intraregional analysis (i.e. within a healthy, heterogeneous, or dense scar region) of DTI voxels did not show any statistically significant difference for any of the DTI parameters (see [Supplementary material online, Figure S6](#)). Intra-case (i.e. in the same heart) and inter-case (i.e. among hearts) comparisons among regions identified two DTI parameters: the FDI and the main eigenvalue, which consistently showed strong statistically significant differences ( $P < 0.0001$ ) for all comparisons; that is, healthy vs. heterogeneous or dense scar; and heterogeneous vs. dense scar (see [Supplementary material online, Figure S7](#)). Therefore, only these two DTI parameters were further associated with each corresponding fibre tract and considered for potential correlation with ventricular arrhythmia inducibility and VT features. Comparison details of the DTI parameters are also shown in the [Supplementary material online](#). Sample representations of FDI and specific FDI comparisons among regions are shown in [Figure 3](#).

## High-resolution scar volumes do not associate with either ventricular tachycardia features or arrhythmia risk

Scar volumes (heterogeneous, dense, or total scar volumes; [Table 1](#)) did not show statistically significant differences between VT inducible

**Table 1** Baseline data, scar and ventricular tachycardia characteristics

	VT inducible (n = 8)	Only VF inducible (n = 4)	Controls (n = 3)
Baseline data			
Male gender, n (%)	8 (100)	4 (100)	2 (66.67)
Weight prior to the VT study (kg)	58 (53–62.25)	61.25 (52–70.38)	55 (52.75–56.5)
LVEF (%)	33.95 (31.08–36.43)	38.9 (33.3–43.63)	52.3 (49.5–54.05)
T1 scar data			
Heterogeneous scar volume (cm <sup>3</sup> )	30.63 (24.73–49.03)	25.77 (20.57–30.9)	
Dense scar volume (cm <sup>3</sup> )	4.53 (3.45–6.39)	6.08 (3.38–9.26)	
Total scar volume (cm <sup>3</sup> )	39.03 (29.52–52.86)	31.15 (23.25–40.16)	
VT features data			
Different SMVT episodes	2.5 (1.75–3.25)		
SMVT cycle length (ms)	213 (205–266)		
SMVT similarity index (%)	98.97 (98.71–99.19)		
SMVT episode duration (s)	132.56 (70.79–251.73)		
Aggressiveness index (%)	25.53 (13.98–38.50)		
VTs CL dispersion per animal (%)	3.3 (1.7–8.9)		
VF inducibility data			
VF aggressiveness index (%)	87.06 (61.92–100)	18.99 (12.97–32.91)	100 (100–100)

Continuous data are expressed as median with interquartile ranges and categorical data as n (%).

CL, cycle length; LVEF, left ventricular ejection fraction; SMVT, sustained monomorphic ventricular tachycardia; VF, ventricular fibrillation; VT, ventricular tachycardia.

(n = 8) and VF-only inducible pigs (n = 4) (Figure 4A, B). Both the median CL of the inducible VT/VTs for each animal and the AI for VT induction did not correlate with scar volumes. Specifically, total scar volumes showed a poor Pearson's correlation coefficient for both median VT CL and AI ( $R^2 = 0.0034$ ;  $P = 0.89$  and  $R^2 = 0.1334$ ,  $P = 0.35$ ; Figure 4C and D, respectively). Heterogeneous and dense scar volumes did not show any correlation with median VT CL and AI either (data not shown). Despite limitations for accurate registration, qualitative analysis of a scar region from a representative histopathologic ventricular section showed that post-contrast R1 sequences could identify scar tissue (see Supplementary material online, Figure S8). Left ventricular ejection fraction did not associate with any of the assessed VT features either (see Supplementary material online, Figure S9).

### Fibre disorganization does associate with ventricular tachycardia features and arrhythmia inducibility

Cardiac tractography was generated using an FA cut-off value of 0.097 and a fibre voxel-to-voxel turning angle cut-off of 40° (see Supplementary material online, Figure S10 and Figure 5A). Unlike the scar volumes and the main eigenvalue ( $P = 0.4202$ ), the FDI corresponding to dense scar regions was significantly higher in VF-only inducible pigs compared with VT inducible animals (0.36, IQR 0.36–0.37 vs. 0.32, 0.26–0.33,  $P = 0.0485$ ; Figure 5B). Importantly, VF-only inducible animals were significantly more sensitive to VF induction than VT inducible animals (AI 19%, IQR 13–32.9% vs. AI 87.1%, 61.9–100%;  $P = 0.0202$ ) and controls (n = 3; AI 100%;  $P = 0.0184$ ; Figure 5C).

The median VT CL for each animal correlated with the FDI within regions of heterogeneous scar ( $R^2 = 0.5320$ ;  $P = 0.0400$ ; Figure 5D). Therefore, the higher the FDI within heterogeneous scar regions, the slower will be the median VT CL. Moreover, the AI for VT induction also correlated with the FDI within dense scar regions ( $R^2 = 0.6048$ ;  $P = 0.0231$ ; Figure 5E). Thus, the higher the FDI within dense scar regions, the lower will be the AI for VT induction. Representative histopathologic ventricular samples also showed myocardial areas with overt fibre disorganization (see Supplementary material online, Figure S8).

A downgrade in resolution to currently reported *in vivo* DTI sequences ( $2 \times 2 \times 8$  mm)<sup>9</sup> yielded large interpolations and an overall decrease of FDI values in all myocardial regions (see Supplementary material online, Figure S11). Only isotropic resolutions of 2 mm<sup>3</sup> partially preserved the statistical trends and associations observed with original resolutions (1.1 mm<sup>3</sup>) (see Supplementary material online, Figures S11 and S12).

### Ventricular tachycardia regions of interest show a high degree of fibre disorganization

In four out of eight VT inducible animals, six VT episodes (median duration 12 min, IQR 6–25 min) were carefully mapped to localize the re-entrant VT circuit. All VT circuits were identified on the left ventricular endocardium after a median of 328 (280–441) represented activation points. Representative VT circuits and registration into the 3D DTI volume are shown in Figure 6A, B and Supplementary material online, Figure S13. The VT ROIs showed a high degree of fibre disorganization compared with healthy myocardial regions (FDI: 0.38, IQR 0.34–0.44 vs. 0.24, 0.20–0.27;  $P = 0.0038$ ; Figure 6C). Further

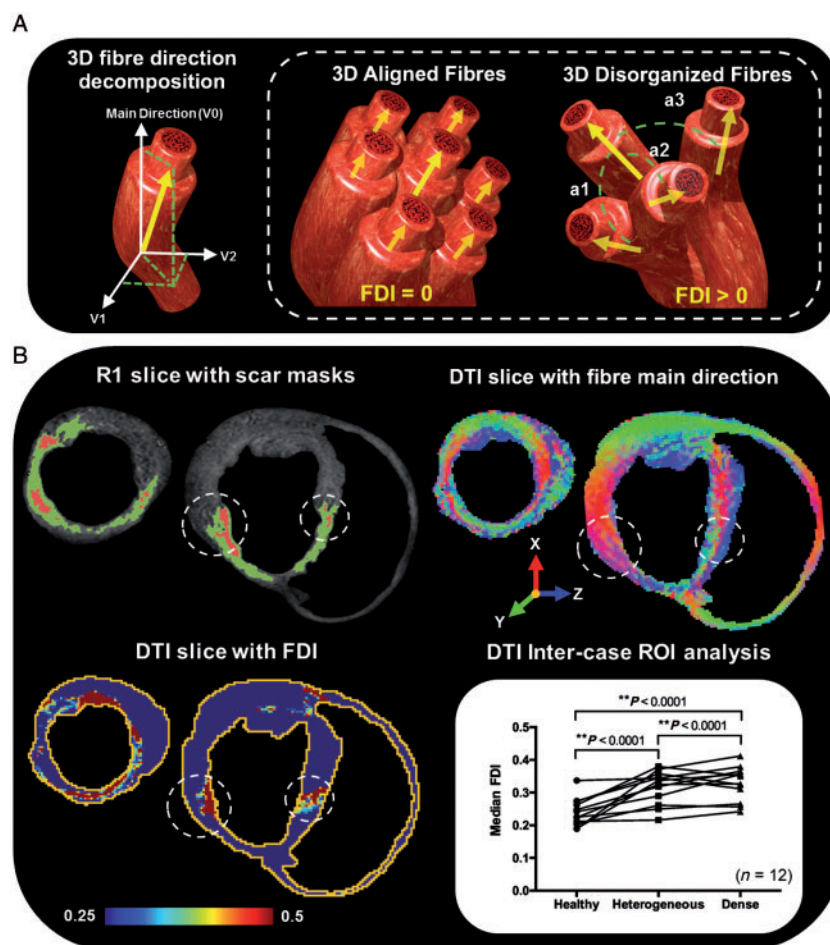


**Figure 3** FDI definition and analysis. (A) Three-dimensional dummy model of a cardiac fibre, including its direction vector (yellow arrow) and its decomposed eigenvectors (on the left). The FDI represents a regional structural disorganization parameter per voxel, which analyses its cumulative 3D angle direction with each neighbouring fibre, relative to a fixed maximum disorganization of  $90^\circ$  in each neighbouring fibre (right panel). (B) Top panels show representative examples of scar distributions in two R1 slices (top left) and colour-coded (red, green, and blue) main fibre direction from the same slices. On the bottom left, colour-coded FDI values from the same slices. White broken circles indicate two specific regions with scar, fibre main direction and colour-coded FDI. Bottom right, median FDI values for healthy, heterogeneous, and dense scar regions. 3D, three-dimensional; DTI, diffusion tensor imaging; FDI, fibre disorganization index; ROI, region of interest.

tissue characterization of the VT ROIs showed that such highly disorganized fibre tracts are mainly within healthy and heterogeneous scar regions (93%, IQR 80.7–99.7%), which supports the need of viable myocardium to sustain re-entry.

## Discussion

We have used high-resolution ex vivo CMR sequences in a pig model of MI to demonstrate that the DTI properties differ between healthy and scar areas. Animal-specific 3D cardiac fibre reconstruction showed that a novel developed DTI-based FDI properly differentiated between VT inducible and VF-only inducible pigs. Re-entrant VT circuits were localized within areas of highly disorganized fibres, mainly composed of viable myocardium. Moreover, the FDI within heterogeneous scar regions was associated with the median VT CL

per animal. Altogether the data presented highlight the importance and potential clinical impact of assessing cardiac fibre disorganization to stratify ventricular arrhythmia risk.

Other clinically relevant parameters like LVEF failed to identify animals with no VT but inducible VF at significantly lower AI values than controls or VT inducible animals (Figure 5C). These results correlate well with clinical data reporting the low specificity and sensitivity of the LVEF as a sole criterion to determine the risk of ventricular arrhythmia.<sup>1,6</sup> Similarly, high-resolution scar characterization and scar volumes did not differentiate between VT inducible and VF-only inducible animals. Moreover, scar volumes did not statistically correlate with VT features either, after a comprehensive study for both VT induction and characterization. Interestingly, our experimental comparisons resemble some clinical endpoints despite results varying among series. Schmidt et al.<sup>14</sup> showed that only the extent of heterogeneous scar regions correlated with SMVT inducibility after

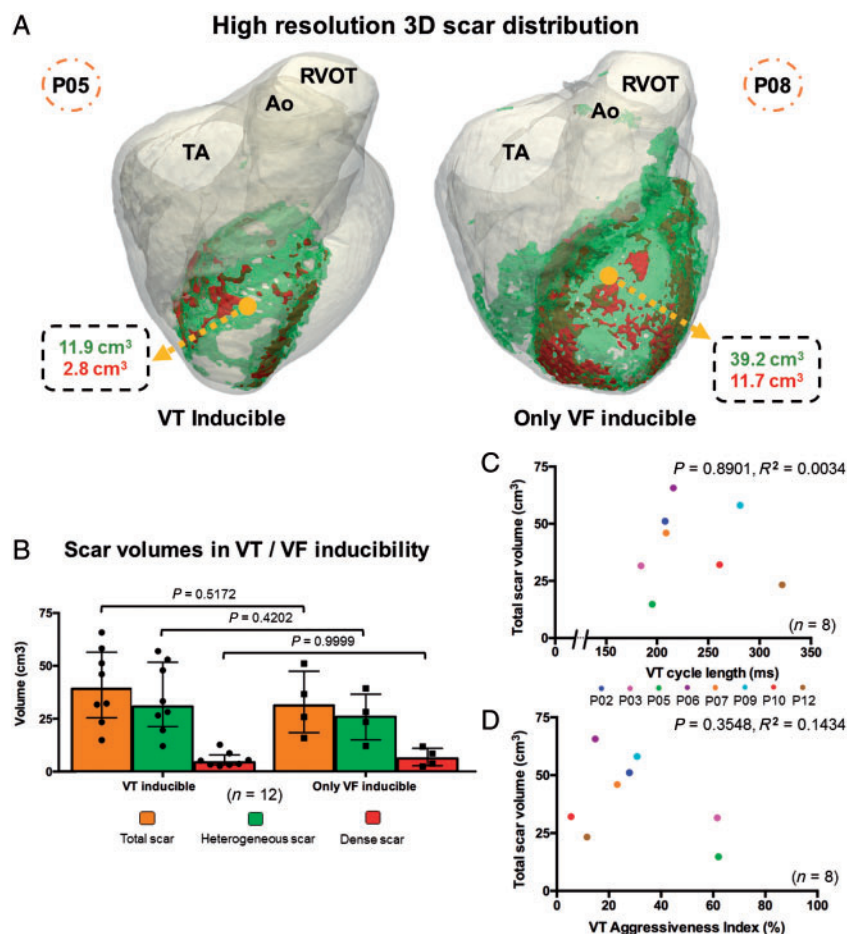


**Figure 4** Scar quantification and implications in ventricular arrhythmia. (A) Three-dimensional scar distribution and quantification from two cases with VT inducible (P05) and VF-only inducible (P08). (B) Scar volumes were not statistically different between VT inducible ( $n = 8$ ) and only VF inducible pigs. Total scar volume correlations with the median animal-specific VT CL (C) and VT induction sensitivity (D). Ao, aorta; CL, cycle length; P02, P03, etc.: pig cases with inducible VT/VTs; RVOT, right ventricular outflow tract; TA, tricuspid annulus; VF, ventricular fibrillation; VT, ventricular tachycardia.

programmed ventricular stimulation. However, they did not address the difference in VF sensitivity between VT and non-VT inducible patients. Also, they acquired LGE-CMR sequences with a spatial resolution of  $1.5 \times 2.4$  mm, and 8-mm slice thickness, which reflects the study limitation in accurately quantifying dense and heterogeneous scar volumes based on the well-known influence of aliasing and partial volume effects.<sup>15</sup> More specifically, the reported scar values of Schmidt *et al.*<sup>14</sup> could have dramatically varied by as much as 70%, from 8 mm to 1.1 mm in slice thickness.<sup>15</sup> The latter reflects the isotropic resolution of the DTI images ( $1.1 \text{ mm}^3$ ) we used to register R1-derived scar regions. Woie *et al.*<sup>16</sup> and Alexandre *et al.*<sup>7</sup> have also addressed the correlation between VT CL and scar extent in two small clinical series; the number of dense scar islands and the scar extent were associated with the mean VT CL of spontaneous episodes during an initial segment of 12–13 VT beats of the first non-sustained or SMVT morphology, recorded by an implantable cardioverter-defibrillator. Such limited analyses of the VT features may have affected the results, since other VT morphologies and longer recording

periods could have yielded different mean VT CL values for comparisons. Another series reporting more extensive evaluation of the VT features during an electrophysiology study did not show statistical differences in mean VT CL values between patients with VT recurrences and no recurrences, although scar extension was significantly larger in patients with recurrences.<sup>17</sup>

Notwithstanding the fact that CMR is not in the clinical guidelines for arrhythmia risk stratification and VT characterization after MI,<sup>1</sup> the use of CMR is evolving and there is a growing body of literature recognizing that scar heterogeneity within the myocardium is especially arrhythmogenic.<sup>12,18</sup> Heterogeneity includes other parameters beyond scar tissue that may be intimately related to it. Thus, fibre disorganization underlying infarct-related remodelling has been previously suggested to contribute to the initiation and maintenance of re-entrant activity after MI. Anter *et al.* have shown in *ex vivo* histopathologic samples that the axis of the VT isthmus was oriented parallel to the myocardial fibres in all the mapped VTs,<sup>4</sup> whereas fibre disorganization was mainly present at the septal and lateral borders



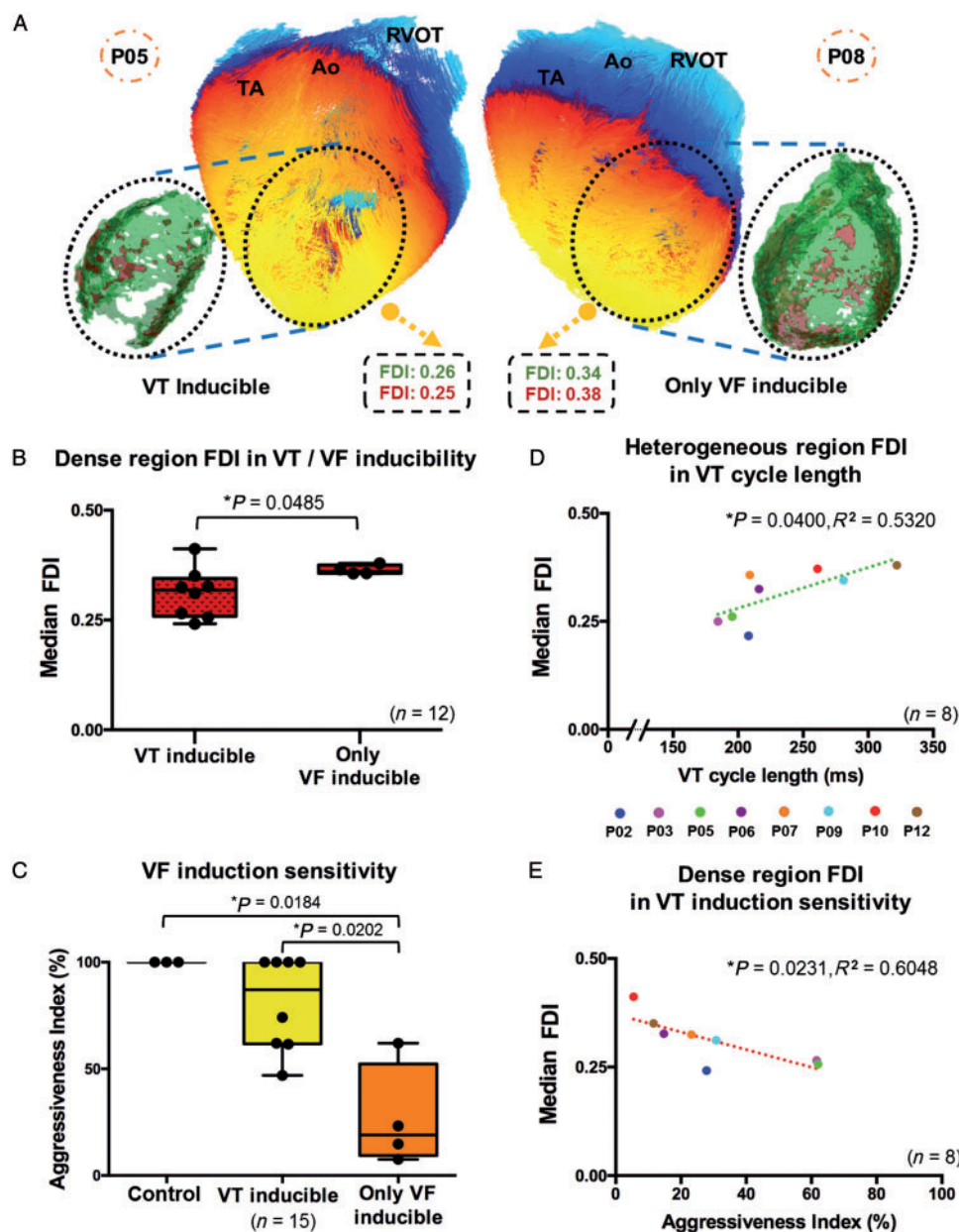


**Figure 5** FDI quantification and implications in ventricular arrhythmia stratification. (A) Two representative cases (P05, P08) of 3D fibre tracts reconstructions and specific FDI values within dense (in red) and heterogeneous (in green) scar areas. (B) VF-only inducible animals showed higher FDI values within dense scar regions than VT inducible pigs. (C) VF inducible animals were significantly more prone to induction (lower values of aggressiveness index) than VT inducible animals and controls. The FDI values significantly correlated with VT CL (D) and VT induction sensitivity (E). 3D, three-dimensional; Ao, aorta; CL, cycle length; FDI, fibre disorganization index; RVOT, right ventricular outflow tract; TA, tricuspid annulus; VF, ventricular fibrillation; VT, ventricular tachycardia.

of the infarct area, which correlates with relatively rapid propagation parallel to the fibre orientation, with much slower propagation perpendicular to the fibre direction; allowing for re-entry maintenance.<sup>8</sup> Here, we showed multimodal imaging registration of scar tissue, fibre distribution, and VT maps to provide a full substrate characterization and electrophysiological assessment after MI, and determine the role of scar and fibre distribution on arrhythmia risk and animal-specific VT features. Fibre tracking criteria identified some viable fibre tracts

within dense scar regions that were highly relevant to VF inducibility. Interestingly, a higher degree of disorganization may facilitate a sudden change in fibre direction and promote the occurrence of unidirectional conduction block and VF initiation.<sup>19</sup> The presence of viable fibres within dense scar areas is supported by our representative histopathology samples (see [Supplementary material online, Figure S8](#)) and previous work by other authors describing highly disorganized surviving fibres within scar areas.<sup>4</sup>

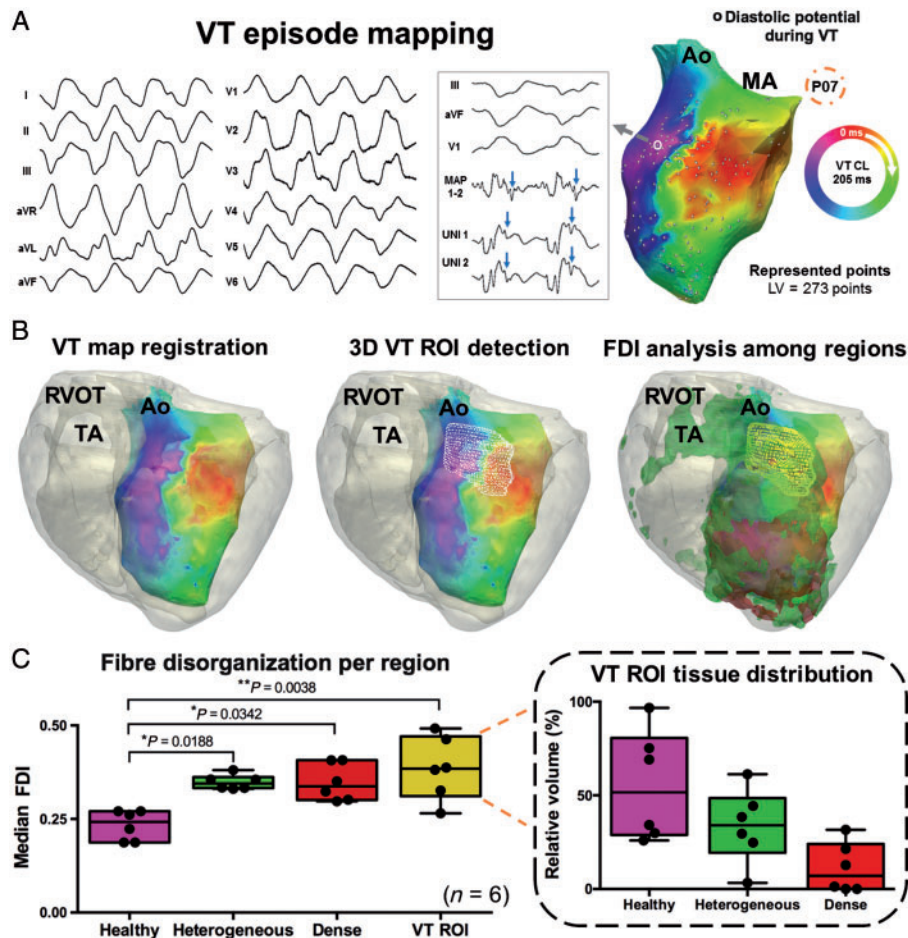


**Figure 6** Fibre disorganization within the VT ROI. (A) ECG and VT activation map from one VT episode (P07). (B) Sample VT ROI generation (Pig07) used for further FDI comparisons among regions. (C) Left panel: FDI values within the VT ROIs show a high degree of disorganization. Right panel: tissue characterization within the VT ROIs. Ao, aorta; CL, cycle length; ECG, electrocardiogram; FDI, fibre disorganization index; LV, left ventricle; MA, mitral annulus; ROI, region of interest; RVOT, right ventricular outflow tract; TA, tricuspid annulus; VT, ventricular tachycardia.

Heterogeneous scar areas have been described to be highly relevant in VT circuits,<sup>12,18</sup> although the underlying fibre disorganization cannot be currently addressed in the clinic using high-resolution imaging. Our data show that fibre disorganization within heterogeneous regions modulates the median animal-specific VT CL, and the newly developed FDI properly assessed 3D fibre disorganization within heterogeneous scar areas. We demonstrated that a high degree of fibre disorganization slows impulse conduction and increases VT CL.<sup>19</sup> Moreover, 3D analysis of the specific VT ROI, comprising entrance and exit sites, showed that fibre disorganization is a relevant parameter modulating VT features. Interestingly, VT ROIs mainly include healthy and heterogeneous scar tissue, which highlights the role of viable myocardial fibres and potential scar-related functional lines of block to generate re-entry.<sup>8</sup>

Fibre orientation has also been incorporated into virtual heart models using a simplified solution that lacks the natural variability in fibre orientation found in histology and DTI studies.<sup>9,10</sup> Moreover, dense scar areas are considered to be non-conductive, with no viable fibre tracts, which might vary depending on the amount of fibrosis

and remaining viable fibres. The latter leads to a potential underestimation of the importance of fibre orientation in assessing the arrhythmia risk and VT features, which in such scenario seem to be determined by the electrophysiological properties assigned to the healthy and heterogeneous scar areas.<sup>18</sup>

## Limitations

Ventricular fibrillation/tachycardia induction using programmed ventricular stimulation cannot be extrapolated to spontaneous arrhythmic events. Additional pacing sites could have increased the chances to induce SMVT in VF-only inducible animals, although the low degree of AI used in such a group make it unlikely that alternative pacing sites would have induced SMVT. The results cannot be extrapolated to patients with VT or VF episodes, which will require new series in patients.

The DTI images were acquired with lower resolution than R1 images, providing higher averaging levels when retrieving structural information. However, scar volumes did not significantly vary after registration and registration errors were negligible (see

Supplementary material online and Figure S5B). We did not address the contribution of haemorrhage and microvascular obstruction at early post-MI stages on chronic scar characterization and DTI parameters. Qualitative histopathologic assessment was only performed in a few myocardial samples. However, FDI data are consistent with previous histopathologic results.<sup>4,20</sup>

## Conclusions

Scar-related cardiac fibre disorganization from DTI sequences allows determination of ventricular arrhythmia risk and VT features in the translational pig model of MI.

## Supplementary material

Supplementary material is available at *Europace* online.

## Acknowledgements

We thank Carlos Xavier-Torres for his contribution in the manual segmentation process of CMR images. We also thank Sandra Muñoz for the analysis of cine images and Dr Stuart Pocock for his statistical advice.

## Funding

The CNIC (Madrid, Spain) is supported by the Ministry of Science, Innovation and Universities and the Pro CNIC Foundation. The CNIC and the BSC (Barcelona, Spain) are Severo Ochoa Centers of Excellence (SEV-2015-0505 and SEV-2011-0067, respectively). This study was supported by grants from Instituto de Salud Carlos III, Fondo Europeo de Desarrollo Regional (RD12/0042/0036, CB16/11/00458), Spanish Ministry of Science, Innovation and Universities (SAF2016-80324-R, PI16/02110, and DTS17/00136), and by the European Commission [ERA-CVD Joint Call (JTC2016/APCIN-ISCIII-2016), grant#AC16/00021]. The study was also partially supported by the Fundación Interhospitalaria para la Investigación Cardiovascular (FIC, Madrid, Spain), the Spanish Society of Cardiology (Dr. Pedro Zarco award) and the Heart Rhythm section of the Spanish Society of Cardiology (DFR). JJ. is supported by R01 Grant HL122352 from the National Heart Lung and Blood Institute, USA National Institutes of Health. J.A.S. is funded by the CompBioMed project, H2020-EU.1.4.1.3 European Union's Horizon 2020 research and innovation programme, grant#675451. D.G.L. has received financial support through the 'la Caixa' Fellowship Grant for Doctoral Studies, 'la Caixa' Banking Foundation, Barcelona, Spain.

**Conflict of interest:** none declared.

## References

- Ibanez B, James S, Agewall S, Antunes MJ, Bucciarelli-Ducci C, Bueno H et al. 2017 ESC Guidelines for the management of acute myocardial infarction in patients presenting with ST-segment elevation: the task force for the management of acute myocardial infarction in patients presenting with ST-segment elevation of the European Society of Cardiology (ESC). *Eur Heart J* 2018;**39**:119–77.
- Priori SG, Blomstrom-Lundqvist C, Mazzanti A, Blom N, Borggrefe M, Camm J et al. 2015 ESC Guidelines for the management of patients with ventricular

- arrhythmias and the prevention of sudden cardiac death: the task force for the management of patients with ventricular arrhythmias and the prevention of sudden cardiac death of the European Society of Cardiology (ESC). Endorsed by: Association for European Paediatric and Congenital Cardiology (AEPIC). *Europace* 2015;**17**:1601–87.
- Luke RA, Saffitz JE. Remodeling of ventricular conduction pathways in healed canine infarct border zones. *J Clin Invest* 1991;**87**:1594–602.
- Tschabrunn CM, Roujol S, Nezafat R, Faulkner-Jones B, Buxton AE, Josephson ME et al. A swine model of infarct-related reentrant ventricular tachycardia: electroanatomic, magnetic resonance, and histopathological characterization. *Heart Rhythm* 2016;**13**:262–73.
- Klem I, Weinsaft JW, Bahnson TD, Hegland D, Kim HW, Hayes B et al. Assessment of myocardial scarring improves risk stratification in patients evaluated for cardiac defibrillator implantation. *J Am Coll Cardiol* 2012;**60**:408–20.
- de Haan S, Meijers TA, Knaapen P, Beek AM, van Rossum AC, Allaart CP. Scar size and characteristics assessed by CMR predict ventricular arrhythmias in ischaemic cardiomyopathy: comparison of previously validated models. *Heart* 2011;**97**:1951–6.
- Alexandre J, Saloux E, Lebon A, Dugue AE, Lemaitre A, Roule V et al. Scar extent as a predictive factor of ventricular tachycardia cycle length after myocardial infarction: implications for implantable cardioverter-defibrillator programming optimization. *Europace* 2014;**16**:220–6.
- Anter E, Tschabrunn CM, Buxton AE, Josephson ME. High-resolution mapping of postinfarction reentrant ventricular tachycardia: electrophysiological characterization of the circuit. *Circulation* 2016;**134**:314–27.
- Mekkaoui C, Jackowski MP, Kostis WJ, Stoeck CT, Thiagalingam A, Reese TG et al. Myocardial scar delineation using diffusion tensor magnetic resonance tractography. *J Am Heart Assoc* 2018;**7**:pii:e007834.
- Pashakhanloo F, Herzka DA, Mori S, Zviman M, Halperin H, Gai N et al. Submillimeter diffusion tensor imaging and late gadolinium enhancement cardiovascular magnetic resonance of chronic myocardial infarction. *J Cardiovasc Magn Reson* 2017;**19**:9.
- Amado LC, Gerber BL, Gupta SN, Rettmann DW, Szarf G, Schock R et al. Accurate and objective infarct sizing by contrast-enhanced magnetic resonance imaging in a canine myocardial infarction model. *J Am Coll Cardiol* 2004;**44**:2383–9.
- Andreu D, Penela D, Acosta J, Fernandez-Armenta J, Perea RJ, Soto-Iglesias D et al. Cardiac magnetic resonance-aided scar dechanneling: influence on acute and long-term outcomes. *Heart Rhythm* 2017;**14**:1121.
- Jiang H, van Zijl PC, Kim J, Pearlson GD, Mori S. DtiStudio: resource program for diffusion tensor computation and fiber bundle tracking. *Comput Methods Programs Biomed* 2006;**81**:106–16.
- Schmidt A, Azevedo CF, Cheng A, Gupta SN, Bluemke DA, Foo TK et al. Infarct tissue heterogeneity by magnetic resonance imaging identifies enhanced cardiac arrhythmia susceptibility in patients with left ventricular dysfunction. *Circulation* 2007;**115**:2006–14.
- Schuler KH, Centola M, George RT, Amado LC, Evers KS, Kitagawa K et al. Characterization of peri-infarct zone heterogeneity by contrast-enhanced multi-detector computed tomography: a comparison with magnetic resonance imaging. *J Am Coll Cardiol* 2009;**53**:1699–707.
- Woie L, Eftestol T, Engan K, Kvaloy JT, Nilsen DW, Orn S. The heart rate of ventricular tachycardia following an old myocardial infarction is inversely related to the size of scarring. *Europace* 2011;**13**:864–8.
- Ávila P, Pérez-David E, Izquierdo M, Rojas-González A, Sánchez-Gómez JM, Ledesma-Carbayo MJ et al. Scar extension measured by magnetic resonance-based signal intensity mapping predicts ventricular tachycardia recurrence after substrate ablation in patients with previous myocardial infarction. *JACC Clin Electrophysiol* 2015;**1**:353–65.
- Arevalo HJ, Vadakkumpadan F, Guallar E, Jebb A, Malamas P, Wu KC et al. Arrhythmia risk stratification of patients after myocardial infarction using personalized heart models. *Nat Commun* 2016;**7**:11437.
- Kleber AG, Rudy Y. Basic mechanisms of cardiac impulse propagation and associated arrhythmias. *Physiol Rev* 2004;**84**:431–88.
- Dillon SM, Allesie MA, Ursell PC, Wit AL. Influences of anisotropic tissue structure on reentrant circuits in the epicardial border zone of subacute canine infarcts. *Circ Res* 1988;**63**:182–206.